Exchange-bias-like coupling in a Cu-diluted-Fe/Tb multilayer

Saumya Mukherjee, Wolfgang Kreuzpaintner, Jochen Stahn, Jian-Guo Zheng, Andreas Bauer, Peter Böni, and Amitesh Paul

Phys. Rev. B **91**, 104419 — Published 20 March 2015

DOI: 10.1103/PhysRevB.91.104419

Exchange-bias-like coupling in a Cu-diluted-Fe/Tb multilayer

Saumya Mukherjee[1,2], Wolfgang Kreuzpaintner[1], Jochen Stahn[2], Jian-Guo Zheng[3], Andreas Bauer[1], Peter Böni[1], and Amitesh Paul[1*]

Technische Universität München, Physik-Department, Lehrstuhl für Neutronenstreuung, James-Franck-Straße 1, D-85748 Garching b. München, Germany

[2] *Laboratory for Neutron Scattering and Imaging, Paul Scherrer Institut, CH-5232 Villigen, Switzerland and*

[3] *Irvine Materials Research Institute, University of California, Irvine, CA 92697-2800, USA*

(Dated: March 13, 2015)

Transition metal–rare earth (TM-RE) Fe/Tb-multilayer systems have been known to show exchange–bias–like shifts in the form of double hysteresis loop (DHL) along and opposite to the field cooling axis. Planar domain walls (DW), with opposite handedness at the interfaces, are held responsible for such DHL. Here, we report on the formation of nanoparticulated Fe layers in the Cu-matrix within a Fe-Cu/Tb multilayer and their eventual low temperature characteristics. AC susceptibility measurements indicate that these *diluted* magnetic clusters have a superspin-glass type of freezing behavior. Eventually, this Fe–cluster/Tb interlayer interaction, which is conjectured to be mediated by the pinned moments within the individual clusters, has helped in increasing the exchange bias field in the system to a high value of ≈1.3 kOe which gradually vanishes around 50 K. Polarized neutron reflectivity confirms a very strong antiferromagnetic (AF) coupling between the individual layers. The magnitude of the magnetic moment of each of the individual Tb or Fe-Cu layer remains similar but due to the strong AF–coupling at the interfaces, the entire ferrimagnetic Fe-Cu/Tb entity flips its direction at a compensation field of around 3.7 kOe. This study shows that magnetic dilution can be an effective way to manipulate the possible domain walls or the clusters in TM and thereby the exchange bias in TM-RE systems.

PACS numbers: 75.30.Gw, 75.70.-i

I. INTRODUCTION

Exchange bias is expected in metal–rare earth (TM-RE) systems at temperatures where the RE exists in the antiferromagnetic (AF) phase [1–4]. RE elements such as Gd, Sm, Dy and Tb have been used regularly to form ferrimagnetic alloys with ferromagnetic (FM) elements, which become coupled to FM alloys to show a sizable exchange bias field $H_{\rm eb}$ [5–7].

It known from earlier studies that AF–coupling at the interface of TM-RE systems helps it in forming planar domain walls at the interface which remain frozen upon cooling [5]. The maximum exchange bias field in such systems is determined by the energy it takes to form a π (bilayer) or 2π (multilayer) planar domain wall (DW) within the softer TM layer. Recently, field cooling of a (TM-RE) Fe/Tb-multilayer system was shown to form a double hysteresis loop (DHL) with exchange–bias–like shifts along and opposite to the field cooling axis, below the ordering temperature of the RE [8]. For the antiferromagnetically aligned (AF-coupled) individual layers of Fe and Tb, there exists a possibility of forming 2π–DWs within the Fe layers, blocked by the anisotropic Tb layers on both sides of Fe. These 2π–DWs were attributed to the origin of the exchange bias. Such a multilayer (unlike a bilayer) consists of regions with a mixture of left–handed DWs and right–handed DWs leading to the observed DHL.

Magnetization reversal of a FM material, at its compensation point, with no external magnetic field is a matter of recent interest. This can be done either by electric fields to manipulate magnetic devices or by optical switching of magnetization using femto–or picosecond pulsed lasers [9]. Manipulation of such DWs in TM-RE multilayers can also be caused upon dilution of the FM system with non–magnetic species. This is because, it is well known that such dilution can help in the formation of magnetic clusters [10], which would have strong influence on the formation of DWs in the system. This dilution, in turn, can adversely affect the exchange coupling in such ferrimagnetic RE-TM systems.

In this paper, we report on field cooling experiments of a diluted–Fe/Tb multilayer showing in-plane magnetic anisotropy. With the motivation of creating Fe clusters within the system we have diluted our Fe/Tb multilayer system with Cu in the Fe layers. Interestingly, we observe no double DHL but an anomalous coupling. The coupling is plausibly mediated by moments pinned within the individual clusters – thus created, as we explore their supermagnetic behavior [11]. Polarized neutron reflectivity confirms a similar behavior of the diluted system as that for an undiluted one reported earlier. The effect of such cluster formation, in the present case, on $H_{\rm eb}$ has been explored and compared with the non-diluted system.

*Corresponding author; Electronic address: amitesh.paul@frm2.tum.de

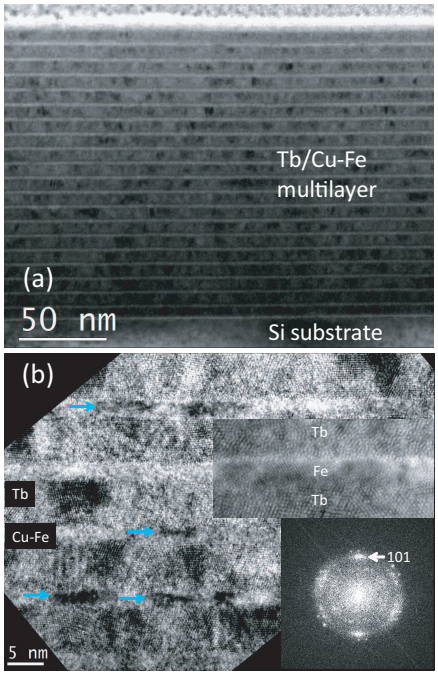

FIG. 1: (a) Cross-sectional bright-field TEM micrograph of the $[Tb/Fe_{0.4}Cu_{0.6}]_{\times N=20}$ multilayer (b) TEM lattice image of the multilayer showing the presence of Fe nanoparticles (indicated by arrows) within the Cu-Fe layers. The inset at the middle-right side is the lattice image of one Fe nanoparticle between Tb layers and the inset at the bottom-right corner is a FFT pattern of the lattice image.

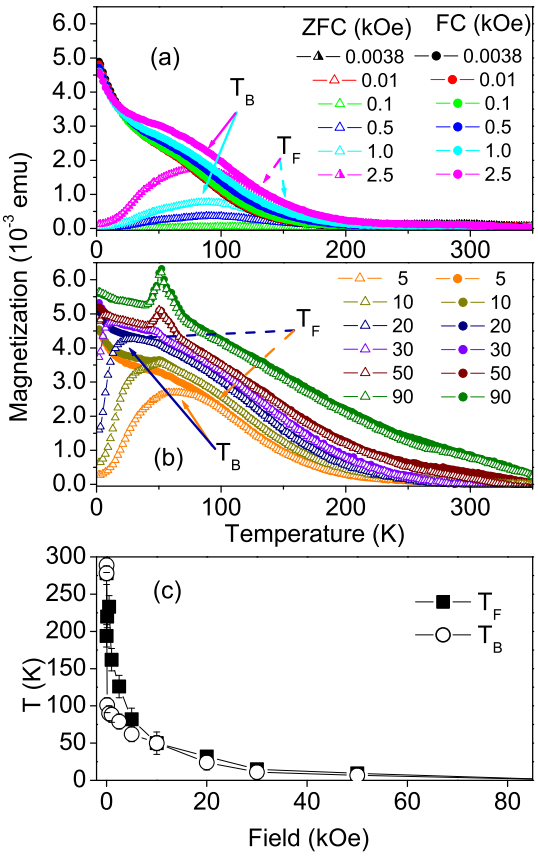

FIG. 2: (Color online) The plot of in-plane magnetization versus temperature after ZFC and FC in 90 kOe measured on heating at various fields (indicated in the figure) (a) 0.0038–2.5 kOe and (b) 5.0–90.0 kOe for $[Tb/Fe_{0.4}Cu_{0.6}]_{\times N=20}$. The peak at 50 K is due to freezing of oxygen in the sample environment. (c) The plots of T_B and T_F as estimated from the above curves with increasing fields of measurement.

II. SAMPLES AND CHARACTERIZATIONS

We have prepared the sample by DC magnetron sputtering using Si(1 0 0) as substrate, of composition $[Tb(6.0\ nm)/Fe_{1-x}Cu_x(3.0\ nm)]_{\times N=20}$. Here x≈0.6 was inferred from x-ray fluorescence spectra for elemental analysis. The Cu dilution was done using a fused target of Fe-Cu in 2:3 proportions. The thickness of the layers are chosen such that the anisotropy is confined to the film plane. During deposition, the Ar pressure in the magnetron sputtering chamber was 3×10^{-3} mbar and the base pressure was 1×10^{-7} mbar.

Cross-sectional transmission electron microscopy (TEM) specimen was prepared using FIB technique in a FEI Quanta 3D SEM/FIB system. TEM experiment was carried out in a FEI/Philips CM-20 TEM with LaB_6 filament operated at 200 kV.

X-ray reflectivity (XRR) measurements on a Siemens D5000 powder diffractometer provide information on the structure of the layers. Conventional in-plane magnetization loops are measured at various temperatures and fields using a physical property measurement system (PPMS).

Polarized neutron reflectivity (PNR) measurements were performed at the reflectometer instrument AMOR in a time of flight (TOF) mode at SINQ, Paul Scherrer Institute (PSI) in Switzerland. An in-plane magnetic field of 10 kOe was used to saturate the FM layer before the samples were cooled in a closed-cycle cryostat.

From the neutron polarization analysis we resolve the different components of the magnetization within the film plane (only the magnetic moment within the sample plane contributes to the scattering). The scattering length densities (SLD) of a specimen are given by the nuclear (ρ_n) and magnetic (ρ_m) components. Two different cross sections were measured namely, non spin flip (NSF) scattering: $(\rho_n \pm \rho_m \cos\phi_A)$ scattering represented by R_{++} and R_{--}. Here + and - signs are used to distinguish the intensity contributions R representing a polarization component parallel or anti-parallel to the guiding field, respectively. Here ϕ_A is the angle between the magnetization M and the applied field H_a.

The low temperature measurements were done using the Selene set-up at AMOR. Here one uses a convergent beam covering a large angular range instead of a collimated beam by using an 4 m long elliptically focusing

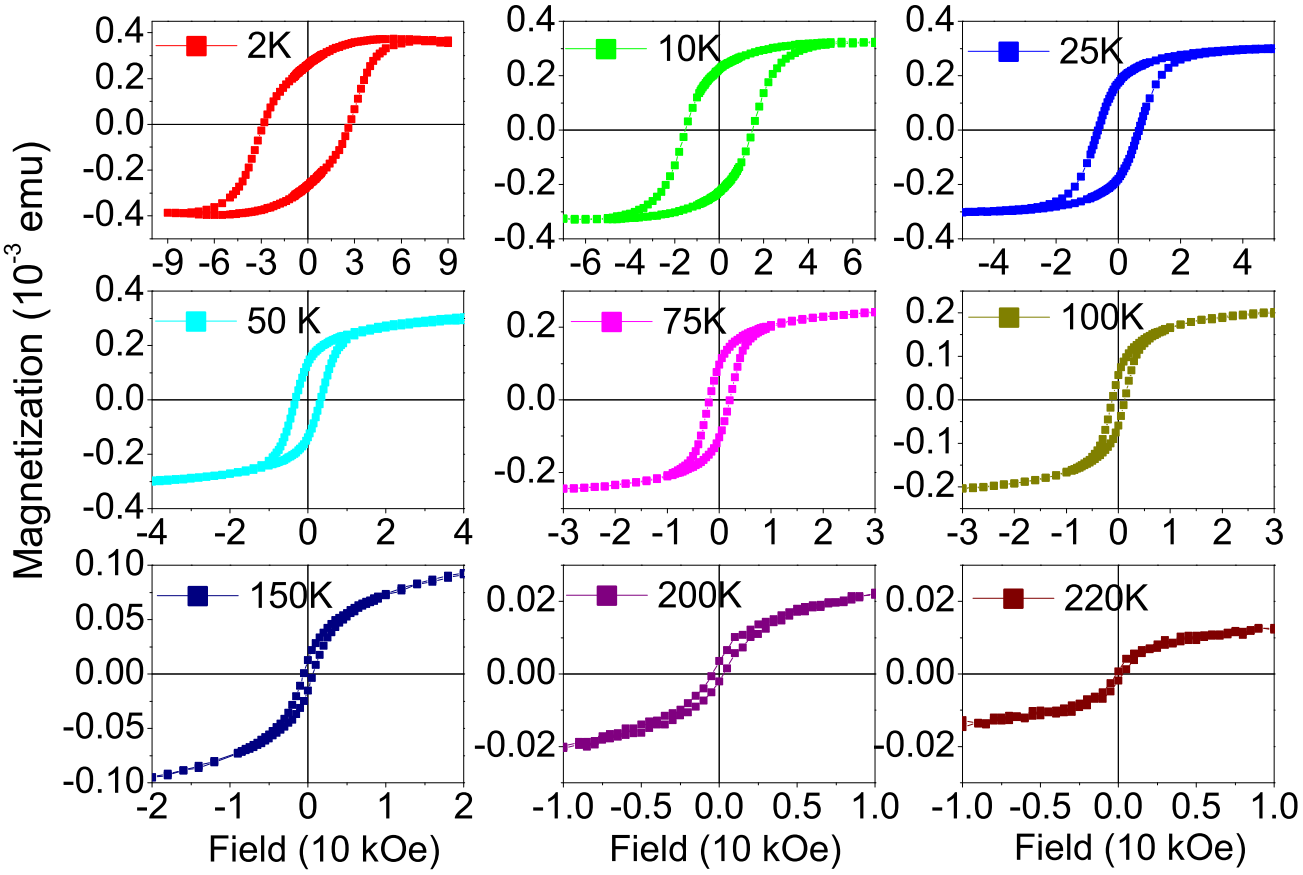

FIG. 3: (Color online) Hysteresis loops for $[Tb/Fe_{0.4}Cu_{0.6}]_{\times N=20}$ sample at various temperatures after field cooling in 90 kOe from 300 K. The loops are corrected for their diamagnetic contributions.

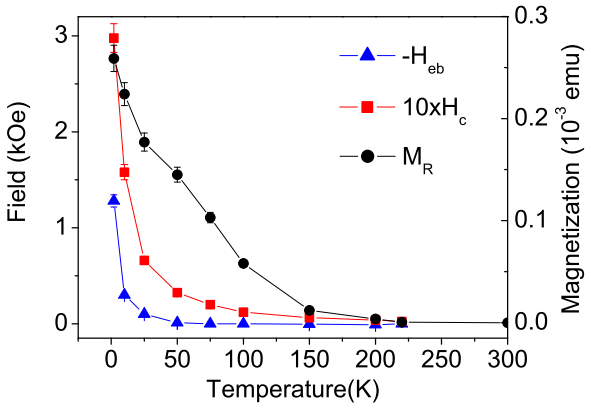

FIG. 4: (Color online) The plot of H_c, H_{eb} (negative bias) and M_R values for $[Tb/Fe_{0.4}Cu_{0.6}]_{\times N=20}$ at various temperatures.

guide element. This essentially increases the intensity by a factor of 10 in the TOF mode [12]. A resolution of 2 mm was obtained using a position sensitive detector (PSD) positioned about 3 m behind the sample to detect the neutrons. The room temperature data was measured using ^{3}He single detectors.

III. RESULTS AND DISCUSSION

A. TEM

Multilayer superlattice was observed in the cross-sectional TEM images as shown in Figure-1-(a and b). Figure-1-(a) is a bright-field TEM micrograph of the Fe-Cu/Tb multilayer with 20 periods grown on a Si substrate. Thin oxide layers on top of the substrate and on top of the last Cu-Fe layer can also be seen. To enhance the contrast of the different layers, the micrograph was

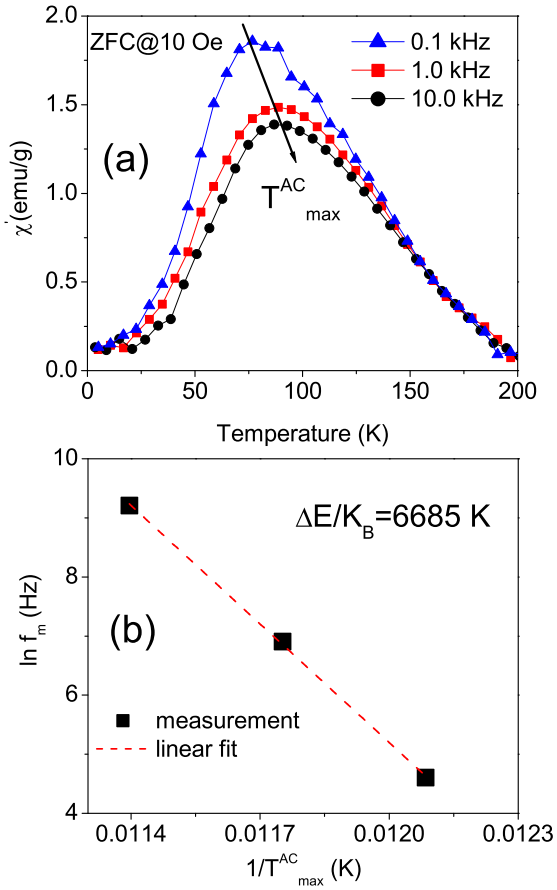

FIG. 5: (Color online) (a) The plot of the ZFC $\chi'=\frac{dM}{dH}$ as a function of temperature for three different AC frequencies for $[Tb/Fe_{0.4}Cu_{0.6}]_{\times N=20}$. (b) Plot of ln f_m versus the inverse of the AC-peak temperature ($1/T^{AC}_{\max}$) and a linear fit to equation 1.

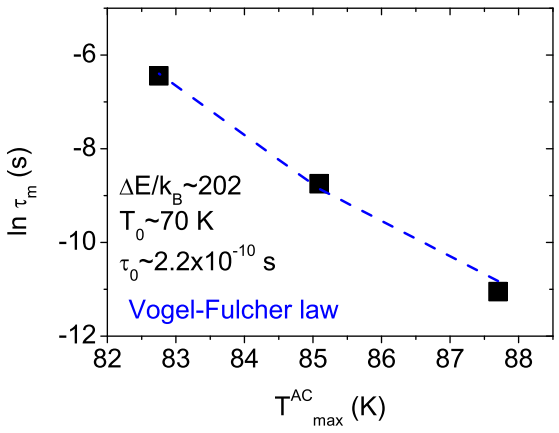

FIG. 6: (Color online) Plot of ln τ_m versus the AC-peak temperature ($T^{AC}_{\max}$) and a fit to equation 3.

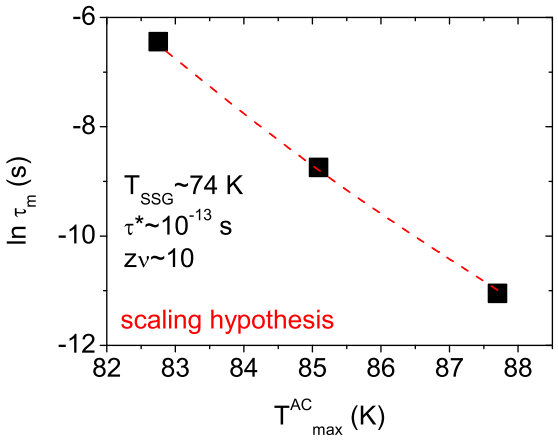

FIG. 7: (Color online) Plot of ln τ_m versus the AC-peak temperature ($T^{AC}_{\max}$) and a fit to equation 5.

taken under an over–focus condition. To determine the nature of each layer, TEM lattice images were recorded and analyzed. Figure-1-(b) shows the typical example of such a lattice image, where the two different layers have average thicknesses of 6.7 nm and 2.2 nm, respectively (which are close to their nominal thicknesses). Lattice fringes are clearly seen in the thicker layer and the interplanar spacings are measured as 0.433 nm,0.307 nm and 0.27 nm, which are well in agreement with Tb, within the measurement error of 1-2%. The inset at the middle-right side of Figure-1-(b) shows an elongated single crystal nanoparticle with two dimensional lattice fringes which are perpendicular to each other with an interplanar lattice spacing of 0.205 nm. These fringes can be explained by (2 0 0) and (0 2 0) planes of Fe instead of the (1 1 1) plane of Cu within the measurement error. The interplanar spacings can also be measured from a fast Fourier transformation (FFT) pattern of the lattice image. The bottom-right inset is the FFT pattern of Figure-1-(b) where there are three rings. The major ring is marked with the index of 101 which corresponds to 0.307 nm. The FFT pattern indicates that the thicker Tb layers are polycrystalline, but display a strong (1 0 1) texture, that is, the (1 0 1) lattice plane of most Tb grains is nearly parallel to the layer interface. The thinner layers are associated with Cu-Fe, but their (amorphous or crystalline) structure cannot be inferred from this TEM image easily. Because the largest lattice spacing of both Cu and Fe is smaller than 0.21 nm, this TEM image does not have the resolution to show lattice fringes with lattice spacing smaller than 0.25 nm because of its imaging condition. Contrast variation, indicated by arrows, imply that these layers are composed of nano-particles in the range of a few nanometers to 10 nm. With improved image condition and higher magnification, these particles show lattice fringes which are consistent with Fe (inset at the middle-right side). It is reasonable to observe iso-

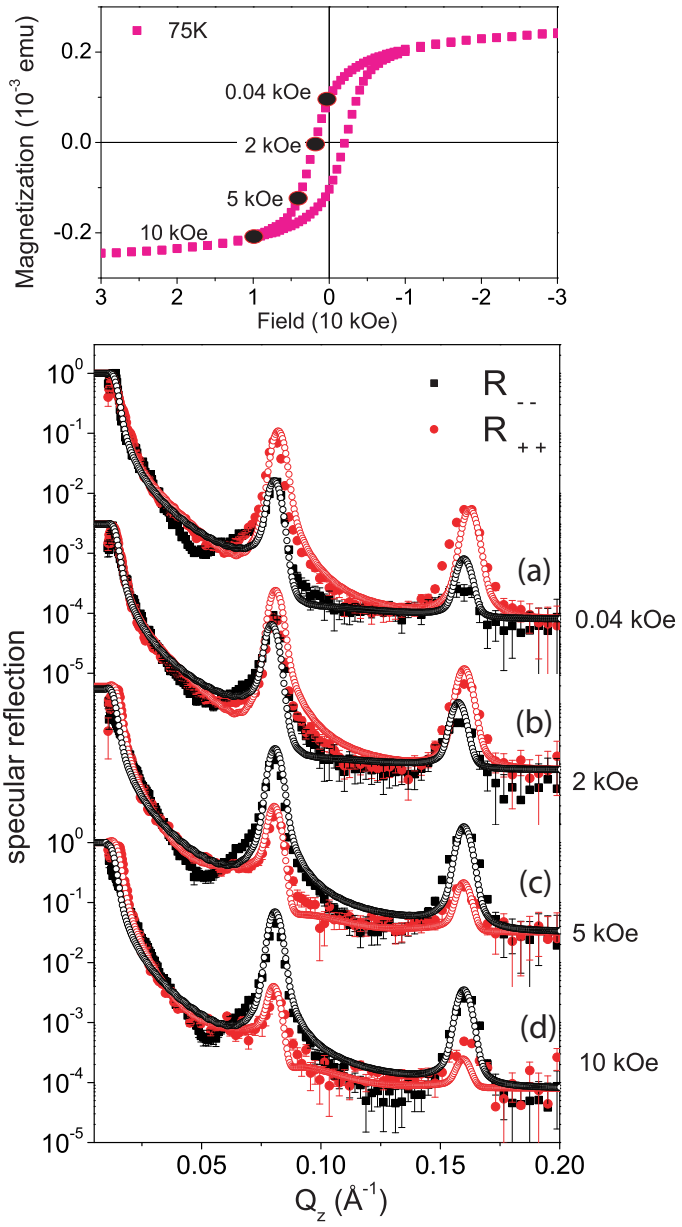

FIG. 8: (Color online) (a–d) PNR measurements at 75 K for spin-up and spin-down polarization for various applied fields H_a along the decreasing branch of the hysteresis loop are plotted versus Q_z along with their best fits (open symbols). The top panel shows the corresponding hysteresis loop. The applied field H_a values for the neutron measurements are marked as circles in the top panel.

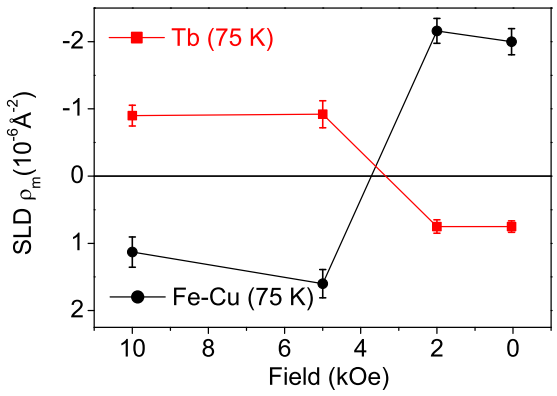

FIG. 9: (Color online) The applied field H_a dependence of ρ_m for the Fe and Tb layers is shown at 75 K. Before the experiment, the multilayer was saturated in a field H_a=–10 kOe.

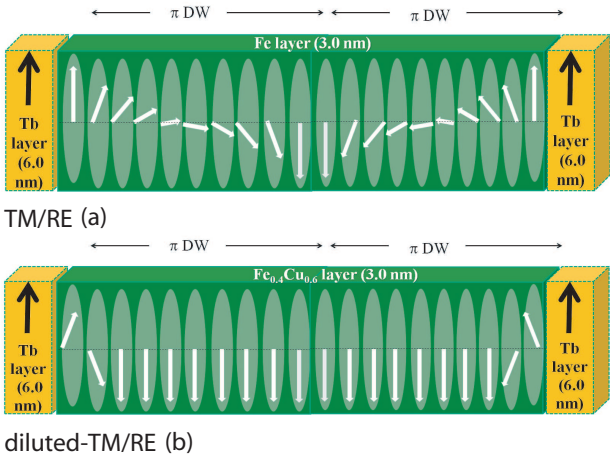

FIG. 10: (Color online) Schematic of the 2π–DWs in (a) non diluted (Ref[8]) and (b) Cu-diluted TM-RE systems.

lated Fe nanoparticles in Cu-Fe layers as Cu is almost insoluble in Fe [13].

B. Magnetization measurements

Figure 2-(a) and (b) show the temperature dependence of the DC magnetization as measured on heating at various fields (starting from 3.8 Oe) after zero field cooled (ZFC) and field cooled (FC) in 90 kOe. A well defined peak can be observed for the ZFC curves (T_B) followed by a furcation point (T_F) with the FC curves. One may note that T_B is conventionally used for blocking in superparamagnetism (SPM) clusters rather than freezing in interacting super–spin–glass (SSG) clusters. Here, we have used T_B to represent the temperatures where we find peaks in the DC magnetization. The T_B and T_F gradually decrease with increasing field values. This is unlike the case for the undiluted system where we observed different variations of T_B and T_F with field [8].

The transition from ferromagnetism to SPM or SSG behavior is generally expected for discrete small clusters where the individual magnetic moments within such clusters are thermally unstable. The SSG state is believed to result from the frustration generated by dipole–dipole interactions among superspins (magnetic moments of nanoparticles) and from disorders in the system (e.g.,

the random distributions of particles, positions, sizes and anisotropy-axis orientations). A further increase of inter-particle interactions can lead to a kind of ferromagnetic domain state or Superferromagnetism (SFM).

If the particle size is sufficiently small, thermal fluctuations dominate above the average blocking/freezing temperature $T_{\rm B}$ and particles can spontaneously switch their magnetization from one easy axis to another. When a small field is applied, the clusters with a lower blocking or freezing temperature (lower than the average blocking/freezing temperature) reach their thermal equilibrium and the sample gains a small net moment. With increasing temperature, more and more clusters become unblocked or unfrozen and this leads to an increase in the net moment. With further increase in temperature, the net moment of the unblocked/unfrozen clusters (superparamagnetic/super–spin–glass) decreases following the Curies's $\frac{1}{T}$ law. This gives rise to a peak in zero field cooled (ZFC) magnetization with temperature. With increasing fields of measurements there is a shift of the blocking/freezing temperature due to a decrease in the energy barrier.

Following the above discussion, one can see that the effect of dilution of Fe with Cu is due to the formation of clusters as we follow the evolution of $T_{\rm B}$ with measurement field in Figure 2-(c). $T_{\rm B}$ decreases with increasing measurement field from 3.8 Oe – 90 kOe. Thus we have a clear indication of formation of Fe clusters in the Cu matrix. These Fe clusters get saturated at ∼50 kOe (comparable with the saturation field of the undiluted system as well as with that of the Tb thin film).

The temperature dependence of the hysteresis loops for the sample $[{\rm Tb/Fe_{0.4}Cu_{0.6}}]_{\times N=20}$ after field cooling in 90 kOe from 300 K is shown in Fig. 3. From the plots, the first thing one can see is that there are no DHLs because the secondary loops are missing even at temperatures as low as 2 K. Here we can confirm that we do not have induced bidomain states. Secondly, along with a very high saturation field (∼ 90 kOe), particularly at low temperatures (lower than 50 K), the hysteresis loops show very large coercive fields. Above 50 K, the saturation field is lower (∼ 30 kOe).

The temperature dependence of $H_{\rm c} = (H_{\rm c}^{+\alpha}–H_{\rm c}^{-\alpha})/2$, where $H_{\rm c}^{+\alpha/-\alpha}$ are the coercive fields for the positive and negative field axes (red squares) and $H_{\rm eb}$ $=(H_{\rm c}^{+\alpha}$ + $H_{\rm c}^{-\alpha})/2$ (blue triangles) for the sample is shown in Fig. 4. One should also note that the 300 K measurements (not shown) exhibits only diamagnetic signal from the substrate without any net magnetization.

Also shown in Fig. 4 is the temperature dependence of the remanent magnetization $M_{\rm R} = (M_{\perp}(H) - M_{\perp}(-H))/2$ (black circles). The change of $M_{\rm R}$ with T indicates a rather monotonic behavior up to $T = 220$ K which corresponds to the blocking/freezing temperature $T_{\rm B}$. Here, $H_{\rm c}$ also vanishes. This is very different from a ferromagnetic behavior in an undiluted sample as has been shown in Ref. 8. Here the $M_{\rm R}$ and $H_{\rm c}$ values go to zero around 220 K, which is typical for a paramagnet. The broadening of the hysteresis loops is caused by the distribution of the cluster sizes leading only to a partial blocking/freezing of the magnetic clusters. Finally, below $T_{\rm B}$ all clusters are blocked or frozen.

For our Cu–diluted–Fe/Tb multilayer system, we have facilitated the formation of nearly monodispersed Fe magnetic clusters embedded in a host matrix of Cu. Most commonly, in such cases, dipolar interactions prevail, while exchange coupling with the establishment of a plausible inter–cluster coupling of the supermoments was also conjectured. Dipolar stray fields between finite-size clusters (superspins), can produce (super)exchange coupling [14]. Spin-glass-like behavior due to strong inter–cluster exchange interactions are common for small separations between clusters [15]. Such a coupling, can be established via Ruderman-Kittel-Kasuya-Yosida (RKKY) interactions between local moments and/or can be of pure dipolar origin. First principle calculations have shown that exchange interaction do not appear to be RKKY-type for smaller separations (less than few nm) between the clusters. They are expected to become RKKY-type only for larger separations [16]. Even more, interaction of the Dzyaloshinsky-Moriya (DM) type has been shown to be enhanced by the presence of nonmagnetic transition-metal impurities [17]. The experimental determination of the magnetic coupling between individual adatoms on surfaces has been demonstrated by recording atomically detailed maps of surface nanostructures using scanning tunnelling spectroscopy with a spin-polarized tip [18].

Thus, the unusually large exchange coupling, that we observe in this system, is conjectured to be mediated by the moments pinned within the individual clusters. The large exchange coupling is plausibly due to the Fe-cluster/Tb interlayer interaction as evidenced by exchange bias vanishing above ≈50 K. The coupling depends on intra-particle blocking/freezing rather than on interlayer interaction.

Earlier, evidences of exchange bias in systems consisting of a FM pinned by a spin–glass was reported experimentally and also simulated theoretically [19, 20]. For a FM layer exchange coupled to bond-diluted pinning layers (which introduced spin disorder in the pinning layer), it was shown by Monte Carlo simulations that with an increasing bond dilution, the spin frustration in the pinning layers would also increase. The pinning layers, thereby, would experience a transition from an AF domain–state to a spin–glass state. This eventually would lead to an enhancement of the bias field.

To determine the type of spin state of non-interacting clusters ensemble, one generally applies the Néel-Arrhenius law [21, 22].

$$f_{\rm m} = f_0 \exp \frac{-\Delta E}{k_{\rm B} T_{\rm B}} \qquad (1)$$

where $\tau_0 = 1/2\pi {\rm f}_0$ is the microscopic limiting relaxation time (∼10^{-9} s) or the inverse of the attempt frequency (f_0) and $\tau_{\rm m}=1/2\pi {\rm f}_{\rm m}$ is the measuring time (∼10^2 s) or inverse of the measuring frequency ($f_{\rm m}$) [23]. $\Delta {\rm E}(={\rm K_A V})$

is the anisotropy energy or activation energy for cluster formation. Here K_A is the anisotropy constant, k_B=1.38×10^{-16} erg/K is the Boltzmann constant and V, the average cluster volume critical for SPM or SSG state at T_B.

The clusters thus formed can be superparamagnetic or super–spin–glass type. A crossover from pure Néel-Brown-type SPM to SSG behavior is possible in randomly distributed nanoparticle systems for high enough density and sufficiently narrow size distribution at a low temperature [24].

In the case of a monodisperse ensemble, the real and the imaginary part of the complex AC susceptibility, $\chi = \chi'$–iχ'', become analytical functions of the AC frequency and temperature. In order to verify such an assumption we perform AC susceptibility $\chi'=\frac{dM}{dH}$ (real part) measurements in our PPMS set-up. The protocol of such a measurement is that after performing ZFC we measure χ' with a temperature sweep for different AC frequencies at an applied field of 10 Oe. We apply an AC field with frequencies 0.1 kHz, 1.0 kHz and 10 kHz. For our diluted sample we find a shift in the ZFC peak (from 82 K to 88 K) as shown in Figure 5-(a) with decreasing frequency. This shift in the AC-peak temperature $T_{\max}^{AC}$ with frequency is typical of SPM or SSG clusters. Note that no such peak shift with frequency was observed in the undiluted system or in the Tb bulk specimen [8].

In the case of a peak shift we need to find whether the clusters are in the SPM (non–interacting spins for diluted samples) regime or in the SSG (interacting super–spins for concentrated samples) state. Generally speaking, these results for the dynamical response are characteristics of blocking or freezing processes, so additional inspection of the thermal and frequency responses are necessary to clarify the nature of the response.

An applied frequency of AC field apparently shifts the blocking or freezing of the clusters to a higher $T_{\max}^{AC}$ value. In other words a variation of f_m in χ'(T) renders a variation in the probe time which allows one to probe the relaxation of particles in different time windows.

It can be mentioned that *non-interacting* SPM particles show large f_m dependence of $T_{\max}^{AC}$ whereas for interacting SSG particles, $T_{\max}^{AC}$ is less f_m dependent. Typically if we have an attempt time $\tau_0 \sim 10^{-8}$–10^{-13} s, we are in the SPM [25] regime of non-interacting spin clusters while any values lower than that refer to super–spin–glass state for interacting spin clusters. We show the variation of frequency (in log scale) with the inverse of temperature $T_{\max}^{AC}$ in Figure 5-(b).

We perform a linear fit to the data and obtain a value of $\Delta E/k_B \approx 6685$ K. This gives

$$\ln(\frac{f_0}{f_m}) = \ln(\frac{\tau_m}{\tau_0}) = \frac{6685}{T_{\max}^{AC}} \quad (2)$$

With f_m ranging from 10^4–10^2 Hz, the estimated value of τ_0 is $\sim 10^{-38}$ s. Incidentally, this refers to an unphysical value. Thus an indication of interacting clusters (enhancing the coupling) cannot be ruled out. Large values of energy are typical of particulate systems, often attributed to dipolar interactions or surface effects in diluted systems [26].

The fitting confirms the interacting nature of these nanoparticles and is in conformity with the slow magnetic relaxation. However, we cannot decide explicitly on the state (SSG/SPM) from the above argument, for which we need to perform either thermometric magnetization measurements or infer from the so-called Cole-Cole plots [27]. Given the sensitivity of our PPMS system and very weak imaginary part (χ'') of the signal from our sample, such thermometric measurements are not expected to be sensitive to the memory effect. Therefore such a confirmation is not possible from the above.

Alternatively, we have also tried to analyze the f_m dependence of $T_{\max}^{AC}$ using the phenomenological Vogel–Fulcher law [28] for *weakly interacting* particles, namely

$$\tau_m = \tau_0 \exp[\frac{\Delta E}{k_B(T_{\max}^{AC} - T_0)}] \quad (3)$$

where T_0 is the characteristic temperature that accounts for the static interaction field of the surrounding particles. We show a plot of ln τ_m versus $T_{\max}^{AC}$ in Figure 6. The values obtained from the fit using equation 3 gives $\Delta E/k_B \sim 202$ with $T_0 \sim 70$ K and $\tau_0 \sim 2.2\times10^{-10}$ s. This indicates that the temperature for the maximum in χ'(T) is due to the freezing of weakly interacting particle moments.

Another useful and sensitive criterion to distinguish between the freezing and the blocking processes is to determine the relative shift of the peak temperature in χ'(T) with frequency and is given by the equation

$$p = \frac{\Delta T_{\max}^{AC}}{\overline{T_{\max}^{AC}}\, \Delta log_{10}(f_m)} \quad (4)$$

where $\overline{T_{\max}^{AC}}$ is the average value of the frequency dependent blocking/freezing temperature determined by the maximum of χ'(T), while $\Delta T_{\max}^{AC}$ denotes the difference between $T_{\max}^{AC}$ measured in the log(f_m) frequency interval [29, 30]. Usually the parameter p assumes values around 0.0045–0.06 for super–spin–glasses and 0.10–0.13 for non-interacting SPM. In our case, the value of p=0.0126 which therefore again indicates an interacting spin glass type of behavior.

Further, if the sample exhibits SSG type of dynamics, the relation of critical slowing down towards the transition temperature T_{SSG} would be expected to follow the scaling hypothesis

$$\tau_m = \tau_*[\frac{T_{\max}^{AC} - T_{SSG}}{T_{SSG}}]^{-z\nu} \quad (5)$$

Here, τ_* is a relaxation time for each nanoparticle, $z\nu$ is the dynamical scaling–critical exponent constant [31] related to the correlation length ξ. In in Figure 7 we plot the variation of τ_m (in log scale) with $T_{\max}^{AC}$. The fit to the equation 5 yields a value of $z\nu \sim 10$ and $\tau_* \sim 10^{-13}$ s,

which are comparable with the typically reported values for super–spin–glass system [30]. Note that a critical exponent value close 1 can be owed to the long-range nature of the dipolar interaction [29] while a larger value as 10, to 3D spin glasses [32]. The high value of $z\nu$ lays within the fragile regime ($5 < z\nu < 11$), common in disordered magnets [33]. In principle, the coupling mechanism (RKKY and/or dipolar) can be further confirmed by investigating the effect of variation in the inter-cluster distances or by the non-equilibrium dynamics (memory effect). Both techniques are beyond the scope of the present work.

C. Polarized neutron measurements

In Figure 8-(a) we show the one dimensional profiles [R_{++}, R_{--}] along Q_z from the NSF channels measured at 75 K along with their fits measured at 0.04, 2, 5 and 10 kOe after field cooling at –10 kOe. The best fits (open symbols) with a simple model of block-potentials yield average scattering length density (SLD) values. They are $\rho_{\rm n}$=4.5×10^{-6}Å^{-2} and $\rho_{\rm m}$=2.3×10^{-6}Å^{-2} for $Fe_{0.4}Cu_{0.6}$ and $\rho_{\rm n}$=3.2×10^{-6}Å^{-2} and $\rho_{\rm m}$=0.6×10^{-6}Å^{-2} for Tb. These values are fairly consistent with the values reported earlier [8], at least for Tb. $Fe_{0.4}Cu_{0.6}$ layers obviously have a reduced $\rho_{\rm m}$ than Fe. Figure 9 shows the field dependence of ρ_m at 75 K which shows a change in the signs of the layer magnetizations at around 3.7 kOe. It may be noted that similar measurements at room temperature did not show any net magnetization in the sample measured at 0.1 kOe which is in agreement with the magnetization data.

The main findings from PNR measurements are i) the magnetic moment of the diluted Fe layers are significantly lower than the non-diluted case. The saturation magnetic moment of Fe at 75 K as estimated from the fits are 1.0±0.1μ_B/atom. ii) The diluted Fe and Tb layers are antiferromagnetically coupled. iii) The antiferromagnetic coupling is seen to persist even at a measurement field of 10 kOe indicating its strength. iv) Interestingly, we find a change of sign for the $\rho_{\rm m}$s of both diluted–Fe and Tb layers with an increasing field. Thus we reach a compensation point of the two sublayers in the multilayer at a field value of ≈3.7 kOe.

In case of the Tb/Fe multilayer system investigated earlier, it was found that the hysteresis loop consists of DHL [8]. Such DHLs were associated with planar DWs. These DWs arose from pinning of the moments by the hard magnetic layer at both ends of the soft magnetic layer which were left and right handed, respectively, giving rise to the shifts in the loops along opposite directions. Such DWs are generally responsible for the observed exchange bias in such systems.

In case of the diluted specimens, no such DHLs are observed. Absence of DHL loops in the hysteresis already indicated that there can be little or no possibility of 2π–DWs in this system unlike the non-diluted one. Thus dilution of magnetic layers by non–magnetic species can help in manipulating the formation of DWs which in turn can affect the exchange biasing effect. A schematic of the DWs in such artificial ferrimagnetic systems is shown in Figure 10-(a) for undiluted and (b) Fe-diluted systems. Magnetization reversal assisted by an external stimuli or by varying the dilution percentage may be made possible on such AF-coupled systems with or without (on diluted or non-diluted) the formation of a 2π–DW at the interfaces.

IV. CONCLUSION

In conclusion, we have studied the exchange coupling in a $[Tb/Fe_{0.4}Cu_{0.6}]_{\times N=20}$ multilayer after field cooling the system in 90 kOe from 300 K to 2 K. Diluted with Cu, an anomalous exchange bias effect was seen with a significant increase in the bias field up to 1.5 kOe and a coercive field of up to 30 kOe at 2 K. The exchange coupling is plausibly attributed to the moments pinned within the individual clusters formed upon Cu dilution. Note that unlike an undiluted system, reported earlier, no DHLs were observed in this case which indicates the absence of bi-domain states. AC-susceptibility measurements show a frequency dependence which can be due to an interaction between the clusters showing SSG type of behavior. The large exchange bias can be plausibly attributed to Fe-cluster/Tb interlayer interaction. PNR data confirms an antiferromagnetic coupling which changes the sign of the individual layer magnetizations but remain strongly antiferromagnetically coupled at least up to 10 kOe. Therefore we have shown that non-magnetic dilution can directly alter the formation of planar DWs in TM-RE AF-coupled systems. The exchange coupling which is determined by the energy it takes to form such DWs or by pinning of individual clusters can thus be manipulated judiciously by varying the percentage of non-magnetic dilution of the TM layers.

Contribution and Acknowledgements The TEM experiments were performed at the Irvine Materials Research Institute (IMRI) at UC Irvine, using instrumentation funded in part by the National Science Foundation Center for Chemistry at the Space-Time Limit under grant no. CHE-0802913. J-G. Z. prepared the cross-sectional TEM specimen using FIB technique, obtained the TEM images, analyzed the TEM results and wrote the TEM related portion. We would like to thank J. Mannhart, A. Herrnberger, T. Mairoser, and A. Schmehl for the collaboration during the course of realizing the sample deposition chamber at the University of Augsburg for the Transregional Collaborative Research Center TRR 80 of the Deutsche Forschungsgemeinschaft. A. B. assisted S. M. in the PPMS measurements. S. M. and W. K. prepared the sample. S. M. and J. S. did the PNR measurements. All authors including P. B. read the manuscript. A. P. planned the work, analyzed the data,

coordinated the work and also wrote the manuscript.

[1] W. C. Cain and M. H. Kryder, J. Appl. Phys. **67**, 5722 (1990).
[2] S. Wuchner, J. C. Toussaint, and J. Voiron, Phys. Rev. B **55**, 17 (1997).
[3] H. J. Santos, F. A. Pinheiro, A. Y. Takeuchi, and L. C. Sampaio, Phys. Rev. B **60**, 1 (1999).
[4] K. Dumesnil, M. Dutheil, C. Dufour, and Ph. Mangin, Phys. Rev. B **62**, 2 (2000).
[5] F. Canet, C. Bellouard, S. Mangin, C. Chatelain, C. Senet, R. Siebrecht, V. Leiner, M. Piecuch, Euro. Phys. Journ. B **34**, 381 (2003).
[6] S. Mangin, C. Marchal, and B. Barbara, Phys. Rev. Lett. **82**, 4336 (1999).
[7] S. Mangin, F. Montaigne, and A. Schuhl, Phys. Rev. B **68**, 140404 (2003).
[8] A. Paul, S. Mukherjee, W. Kreuzpaintner, P. Böni, Phys. Rev. B **89**, 144415 (2014).
[9] S. Mangin, M. Gottwald, C-H. Lambert, D. Steil, V. Uhlr, L. Pang, M. Hehn, S. Alebrand, M. Cinchetti, G. Malinowski, Y. Fainman, M. Aeschlimann, E. E. Fullerton, Nature Mater. **13**, 286 (2014).
[10] R. D. Noce, O. D. M. Gomes, S. D. de Magalhés, W. Wolf, R. B. Guimarés, A. C. de Castro, M. J. M. Pires, W. A. A. Macedo, D. Givord, and V. M. T. S. Barthem, J. Appl. Phys. **106**, 093907 (2009).
[11] S. Bedanta, W. Kleemann, J. Phys. D: Appl. Phys., **42**, 013001 (2009).
[12] J. Stahn, T. Panzner, U. Filges, C. Marcelot, P. Böni, Nucl. Instrum. Method A **634**, S12S16 (2011).
[13] S. Cammelli, C. Degueldre, A. Cervellino, S. Abolhassani, G. Kuri, J. Bertsch, D. Lützenkirchen-Hecht, R. Frahm, Nucl. Instrum. Method B **268**, 632637 (2010).
[14] W. Kleemann, O. Petracic, and Ch. Binek, G. N. Kakazei, Yu. G. Pogorelov, and J. B. Sousa, S. Cardoso and P. P. Freitas, Phys. Rev. B **63**, 134423 (2001).
[15] Y. Qiang, R. F. Sabiryanov, S. S. Jaswal, Y. Liu, H. Haberland, and D. J. Sellmyer, Phys. Rev. B **66**, 064404 (2002).
[16] R. Skomski, R. F. Sabiryanov, and S. S. Jaswal, J. Appl. Phys. **87**, 5890 (2000).
[17] J. J. Prejean, M. J. Joliclerc, and P. Monod, J. Physique **41**, 427 (1980).
[18] L. Zohu, J. Wiebe, S. Lounis, E. Vedemenko, F. Meier, S. Blügel, P. H. Dederichs and R. Wiesendanger, Nature Phys. **6**, 187 (2010).
[19] M. Ali, P. Adie, C. H. Marrows, D. Greig, B. J. Hickey, and R. L. Stamps, Nat. Mater. **6**, 70 (2007).
[20] X. Zhan, Z. Mao, X. Xu, and X. Chen, W. Kleemann, Phys. Rev. B **86**, 020407(R) (2012).
[21] L. Néel, Ann. Geophys. **5**, 99 (1949).
[22] W. F. Brown, Jr., Phys. Rev. **130**, 1677 (1963).
[23] M. Knobel, W. C. Nunes, L. M. Socolovsky, E. De Biasi, J. M. Vargas, and J. C. Denardin, J. Nanosci. Nanotechnol. **8**, 2836 (2008).
[24] C. Djurberg, P. Svedlindh, P. Nordblad, M. F. Hansen, F. Bødker, and S. Mørup, Phys. Rev. Lett. **79**, 5154 (1997).
[25] M. Thakur, M. Patra, S. Majumdar, and S. Giri, J. Appl. Phys. **105**, 073905 (2009).
[26] F. Luis, F. Petroff, J. M. Torres, L. M. García, J. Bartolomé, J. Carrey, and A. Vaurès, Phys. Rev. Lett. **88**, 217205 (2002).
[27] O. Petracic, X. Chen, S. Bedanta, W. Kleemann, S. Sahoo, S. Cardoso, and P. P. Freitas, J. Magn. Magn. Mater. **300**, 1 (2006).
[28] M. Cyrot, Physics Letters, **83 A**, 275 (1981); H. Vogel, Phys. Z. **22**, 645 (1921); G. S. Fulcher, J. Am. Ceram. Soc. **8**, 339 (1925).
[29] J. A. Mydosh, Spin Glasses: An Experimental Introduction (Taylor and Francis, London, 1994) pp. 66 67.
[30] Adriana Zelenáková, Vladimir Zelenák, Ŝtefan Michalík, Jozef Kovác, and Mark W. Meisel, Phys. Rev. B **89**, 104417 (2014).
[31] K. Hiroi, K. Komatsu, and T. Sato, Phys. Rev. B **83**, 224423 (2011).
[32] K. Gunnarsson, P. Svedlindh, P. Nordblad, L. Lundgren, H. Aruga, and A. Ito, Phys. Rev. Lett. **61**, 754 (1988).
[33] J. A. De Toro, M. A. L´opez de la Torre, J. M. Riveiro, J. Bland, J. P. Goff, and M. F. Thomas, Phys. Rev. B, **91**, 8396 (2002).